Digital Object Identifier 00.0000/ACCESS.2026.DOI

Local Aspects of Polar Magneto-Optical Kerr Effect (MOKE) Magnetometry

IVAN SOLDATOV[1], AMAN SINGH[1], VOLKER NEU.[1], and RUDOLF SCHÄFER.[1,2], (Senior Member, IEEE)

[1]Leibniz Institute for Solid State and Materials Research (IFW) Dresden, Helmholtzstrasse 20, D-01069 Dresden, Germany
[2]Institute for Materials Science, TU Dresden, 01062 Dresden, Germany

R. Schäfer (email: r.schaefer at ifw-dresden.de).

ABSTRACT Magnetic hysteresis curves, measured by MOKE magnetometry, should be interpreted with caution, as their recorded local characteristics can vary significantly depending on the sample location. Therefore, conclusions about sample parameters (such as coercive field strength) do not necessarily reflect the characteristics of the entire sample. This is especially true if MOKE magnetometry is performed with probing spot sizes very much smaller than some characteristic domain size or sample area covered by domain nuclei. In this article this is demonstrated for magnetic films with perpendicular anisotropy by measuring polar MOKE loops in a wide-field Kerr microscope. On the examples of Co/Pt films with different domain nucleation behaviour we show that the locally measured coercive field may vary up to several ten percent and that the spot size, from which the Kerr signal is recorded, needs to comprise a critical number of at least domain nuclei to obtain coercivities that are relevant for the whole specimen. We furthermore demonstrate that the speed of loop recording strongly matters in perpendicular media due to domain wall creeping effects.

INDEX TERMS MOKE magnetometry, magneto-optical Kerr effect, magnetic domains, magneto-optical Kerr microscopy, magnetic hysteresis.

I. INTRODUCTION

MOKE magnetometry, i.e. the optical measurement of magnetization curves using the magneto-optical Kerr effect (MOKE)[1], is usually performed in commercial or home-built facilities in which the Kerr signal of a micrometer-sized laser beam that is focused on and then reflected from the sample, is recorded as a function of the applied magnetic field [1], [2]. This leads to local magnetic hysteresis curves corresponding to the spot size of the laser. Spatially resolved measurements are possible by scanning the laser beam over the sample. Alternatively, MOKE magnetometry can be performed in a wide-field Kerr microscope [3]. Such microscopes are primarily used for imaging magnetic domains, but also serve as optical magnetometers by plotting the intensity of a selected region in the Kerr image as a function of field [4]. The advantage of this combined method is that the domains that determine the hysteresis curve are simultaneously imaged, allowing a straightforward physical interpretation of the magnetization mechanisms underlying the loops.

With MOKE magnetometry, exceptionally high sensitivity can be achieved (Chapter 4.3.4 in [5], [6]) when high-frequency noise is suppressed by a lock-in amplifier technique. Although long-term drift remains a limiting factor, this approach makes this type of magnetometry the method of choice for hysteresis studies of thin and ultra-thin magnetic film samples. There are, however, some general critical points that need to be taken into account [3]:

- In contrast to SQUID- or vibrating sample magnetometry, magnetisation cannot be measured quantitatively with MOKE magnetometry. Normally, the Kerr signal is plotted in arbitrary units, often incorrectly referred to as “Kerr rotation". Rather, it is advisable to represent the magnetization in reduced units M/M_s by normalizing the Kerr signal to the signal at saturation.
- Optical components of the magnetometer, such as objective lenses, can introduce an additional spurious polarization rotation due to the magneto-optical Faraday

[1]It has become common to refer to the optical magnetometry technique by the acronym MOKE, which actually makes little sense

effect when they are exposed to the applied magnetic field or the stray field emanating from the edges of a magnetized (bulk) sample or from grain boundaries [7], [8] [2]. This can lead to superimposed signals that become apparent from to non-constant loops at saturation. If the superimposed signal is linear in the applied field, it can be easily subtracted. For non-linear Faraday contributions, it is advisable to measure these separately by recording the intensity at a non-magnetic location in the image. They can be compensated for in-situ during the loop measurement by automated rotation of the analyzer [4]. This method is well suited for (polar) Faraday contributions caused by magnetic field components along the objective axis. Alternatively, lensless reflection objectives can be used. For magnetometry in in-plane fields, Faraday contributions can be well compensated by recording the loops in a pure in-plane sensitivity-only mode [7], [9]. This not only suppresses the polar Kerr contrast of the sample, but also eliminates polar Faraday signals.

- If MOKE magnetometry is performed on metallic optically thick samples (including *bulk* materials or *thick* films), one must be aware that the Kerr effect only senses the magnetization within a limited optical penetration depth (typically of the order of 20 nm for visible light, depending on the wavelength, angle of incidence, and the possible presence of non-magnetic capping layers). The loop is therefore essentially generated by the surface domains. During the magnetization process, the surface closure domains are rearranged to avoid net magnetization components perpendicular to the surface, while the total net magnetization of the sample along the measurement field continues to increase with the field. Up to the “knee” of the hysteresis loop, this can lead to reduced or even negative surface permeabilities [7], [10]. Such effects are interesting in themselves, but the surface loops are by no means representative of the entire sample. For ultrathin magnetic films magnetic films such effects do not occur.
- Regardless of whether bulk or film samples are measured, there is another aspect that must be taken into account in any case: MOKE magnetometry records local hysteresis loops, defined by the field of view or by a selected region of interest (ROI). Such local loops can vary greatly from location to location and from an integral loop measured on the entire sample. In ref. [11] it was shown that even a simple permalloy (80% Ni-Fe) film element with in-plane magnetization, which exhibits a coercivity-free linear overall longitudinal MOKE loop, shows a large number of different local loops with curves of high and low coercivity and even inverted loops (reverse switching). They can be regarded as hysterons in the sense of the Preisach model, which add up to an overall loop. The reason for this phenomenon is the fact that in MOKE magnetometry the signal is always plotted as a function of the external applied magnetic field, while the actual switching is driven by the local *internal* magnetic field, which is strongly modified by local demagnetizing effects and dipolar interactions from the surrounding magnetic landscape.

[2]Such stray field effects, caused by a magnetized specimen itself, were already identified in an early work by *Rave and Hubert* [8] and they were more thoroughly investigated later by *Marco et al.* [7]. In the latter work the first paper was overlooked by mistake

In this article we address this last aspect of local magnetometry again, but now considering extended films with perpendicular magnetic anisotropy (PMA) that are measured in out-of-plane fields. Here the internal magnetic field, being the applied field minus the demagnetization field, is not location dependent. Nevertheless, it turns out that local MOKE loops may differ significantly from global loops depending on the domain size and domain nucleation behaviour in the film as will be elaborated in Sect. III.

II. EXPERIMENTAL

Three PMA thin films were prepared by DC magnetron sputtering: **S1**: Cr_2O_3(5)/Co(0.7)/Pt(2), **S2**: Ta(3)/Pt(5)/Co(0.7)/Ta(3)/Pt(1), **S3**: Ta(10)/Pt(2)/$[Co(0.5)/Pt(0.9)]_5$/Pt(2)/Au(5). The numbers in brackets are given in manometers. The differences in the stack structure and film thickness result in different characteristic domain sizes near the switching field and domain nucleation center densities as shown in Fig.1. The substrates were cut in pieces of approx. 8×8 and 10×10 mm to obtain the samples for MOKE microscopy and magnetometry.

The MOKE hysteresis loops and corresponding domain images were recorded in a wide field magneto-optical Kerr microscope, equipped with image processing for contrast enhancement and a solenoid that allows to generate magnetic fields up to $\mu_0 H$ =100 mT perpendicular to the film plane (i.e. along the objective lens). A 1.25×/0.03 (magnification / numerical aperture) objective lens was used to cover as large sample areas as possible. By using camera adapters with 1.0× and 0.63× magnification factors, the microscope image was projected on the chip of a CMOS camera (Hamamatsu C11440-36U) resulting in rectangular images with a size of 960×600 pixels, which corresponds to approx. $9.34 \times 9.34\,\mu m^2$ and $14.8 \times 14.8\,\mu m^2$ sample areas per image pixel, respectively. For “global" loop measurements the averaged Kerr intensity of an entire image was plotted as a function of the magnetic field. "Local" curves were obtained by dividing the image into a matrix of square elements and plotting the intensities of these elements. To do this, several neighbouring pixels on the camera sensor (2×2, 4×4, 10×10, etc.) were combined into virtual pixels of various sizes (pixel binning), which we address as ROIs in the following. The magnetization reversal curves (Section. III) were obtained using a quasistatic domain imaging approach, in which the magnetic field was varied in 1000 discrete steps

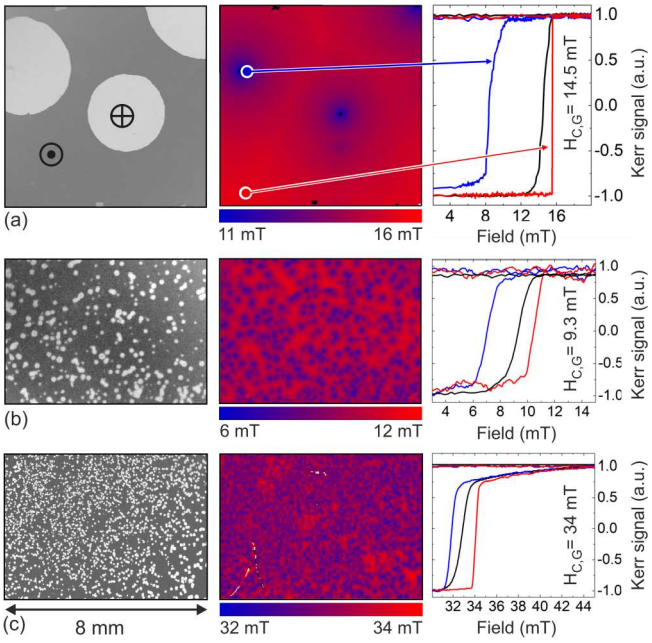


FIGURE 1. Domains in Co/Pt films with different nuclei number (left column), the spatial distribution of the local coercive fields (middle column), and corresponding MOKE loops measured on the whole specimen (black) and at two locations with the lowest (blue) and highest (red) coercive field values (right column): **(a)** sample **S1** with large domains, **(b)** sample **S2** with medium domains, **(c)** sample **S3** with small domains. The ROI size for the analysis is $18 \times 18\ \mu m^2$ for (a) and $29.6 \times 29.6\ \mu m^2$ for (b) and (c), with the whole image size being 600×600 pixels for (a) and 600×800 pixels for (b) and (c)

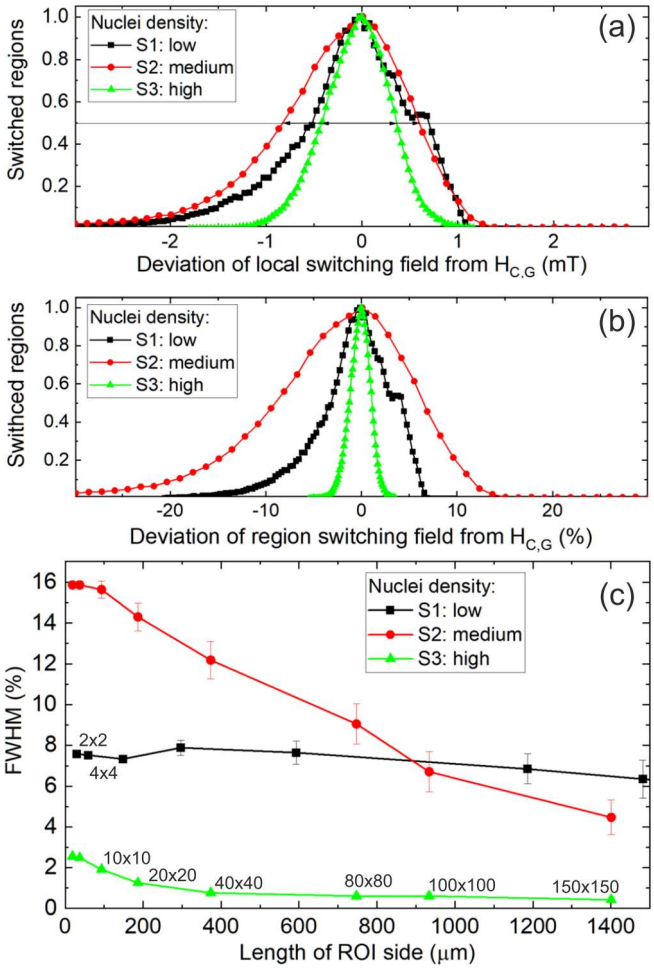


FIGURE 2. Distribution of magnetization switching within a local region of interest (2×2 pixels), normalized to the maximum value as a function of **(a)** absolute and **(b)** relative (in %) field deviation from the global coercive field $H_{C,G}$ for various characteristic domain types (large, middle and small) in Co/Pt. **(c)** FWHM of the magnetization switching distribution as a function of the region (ROI) size used for the analysis and defined by pixel binning.

with a measurement time of approximately 1 second per point (averaging of 16 frames with 56.8 ms exposure time and 200 ms setup stabilization time). To investigate the dynamics (Section.IV), magnetization curves were recorded without frame averaging at a short exposure time (approx. 2 ms) under an applied triangular AC magnetic field. The Co/Pt samples were studied under polar Kerr contrast conditions, while the longitudinal Kerr effect was used to study a nickel film for comparison.

III. ANALYSIS OF LOCAL HYSTERESIS LOOPS

To investigate the difference in the local and global hysteresis behaviour of the three samples, the magnetic field dependence of the underlying domains and their nucleation behaviour were evaluated. The sheared, non-rectangular shape of the global loops (right column in Fig.1) arises from the spatial averaging of scattered local switching events. This macro-behavior is typical for systems with perpendicular magnetic anisotropy, where local pinning on structural defects stretches the global switching curve [12], [13].

Sample **S1**, consisting of a single-layer Co/Pt film and being completely displayed in Fig.1a, is remagnetized by the nucleation of only a few bubble domains within the whole sample area of $8 \times 8\,\mathrm{mm}^2$ that grow by domain wall motion as the field changes. This results in a strong variation of the coercivity, H_c, when measured locally within ROIs with a size of 2×2 pixels (approximately $30 \times 30\ \mu m^2$). If a ROI is located near a nucleation site, it is passed by the wall immediately after nucleation, while an ROI located further away is only reached by a wall later on, leading to different switching fields for different ROIs. The coercivity of such local loops can actually deviate by several ten percent from the global coercivity ($H_{C,G}$), which is immediately evident from the colour plot in Fig.1a. This variation is also seen in the normalized distribution of the local coercive fields displayed by the black curves in Fig.2 (a) and (b) for the same sample. The full width at half maximum (FWHM) of this distribution is ∼1.23 mT, which corresponds to 8% of the global sample coercive field value of 16.3 mT. The asymmetry in the FWHM distribution for sample **S1** is associated with an asymetrical nucleation of the bubble domains as was also observed in Ref. [14].

Sample **S2** demonstrates a substantially larger number of nuclei (around 300 within the whole sample area), as shown in Fig.1b. Nevertheless, the distribution of the local coercivity remains broad as can be seen from the colour plot in Fig.1b and the red curve in Fig.2a. When the distribution is shown

as a percentage of the global $H_{C,G}$ (Fig.2b), the broadening appears even larger compared to the sample with only three nuclei, since the absolute $H_{C,G}$ value of sample **S2** is slightly lower.

The wide distributions for these two samples are not surprising: if we assume that each bubble nucleus occupies one image pixel, even in case of sample **S2** the area occupied by the nuclei immediately after their appearance is only 0.052% (300 one-pixel bubbles within the 960×600 pixel image) of the total sample area. Thus, the probability of encountering a bubble within the randomly located 2×2 pixels ROI during the local analysis is correspondingly small. As already explained for sample **S1**, the magnetization within an ROI without a nucleus only switches when a nucleated bubbles in the vicinity grows and covers the ROI by wall motion, resulting in a large H_c difference between ROIs located near a nucleus and those further away from the nucleus

The coercivity variance improves slightly when the number of nuclei within the entire sample area exceeds 10^3 nuclei. This is the case for sample **S3** shown in Fig.1(c), for which approx. 1500 nuclei appear upon magnetization reversal. Although the ratio of the sample area occupied by nuclei still remains rather small (around 0.3 % of the total sample area), the FWHM of the coercive field distribution has decreased compared to the other two samples (see the green curves in Fig.2 a and b), though not drastically if considered in absolute field values.

However, significant differences between the three samples can be observed when we increase the size of the ROIs, i.e., employ different pixel binning for the hysteresis analysis, and plot the FWHM of the local H_c distribution (normalized to global $H_{C,G}$) as a function of ROI size (Fig. 2c). For sample **S1** with 3 nuclei (black curve in Fig. 2c), enlarging the ROI results in almost no change in width of the local H_c distribution. For sample **S2** with moderate nuclei numbers (red curve in Fig. 2c) it only leads to a slow decrease in the FWHM values. Even with a ROI size of 1/8 of the total sample area, there is still a large variation in local coercive field values (around 5 % of global $H_{C,G}$). In contrast, in sample **S3** with a large number of nuclei (green curve in Fig. 2c), a 20-fold increase in ROI size (pixel binning from 2×2 to 40×40) leads already to a rather sharp decrease in the variation of local H_c, followed by a slow decrease for larger ROIs.

This approach allows us to estimate the relationship between the number of nuclei and the minimum field of view required for a reasonable assessment of global sample properties based on local observations. The nuclei densities for the three samples are 0.46, 6.8, and 32 nuclei/mm^2, respectively. For the sample with the largest number of nuclei, a decently narrow distribution of the local H_c (below 1 % of global $H_{C,G}$) is observed at a ROI size of 373×373 μm^2 (40×40 pixels), which corresponds to approximately 4.5 nuclei within this ROI. For the sample with a medium number of nuclei, a similar decrease in coercivity variation might be achieved at $1.8 \times 1.8\, mm^2$ (200×200 pixels), which

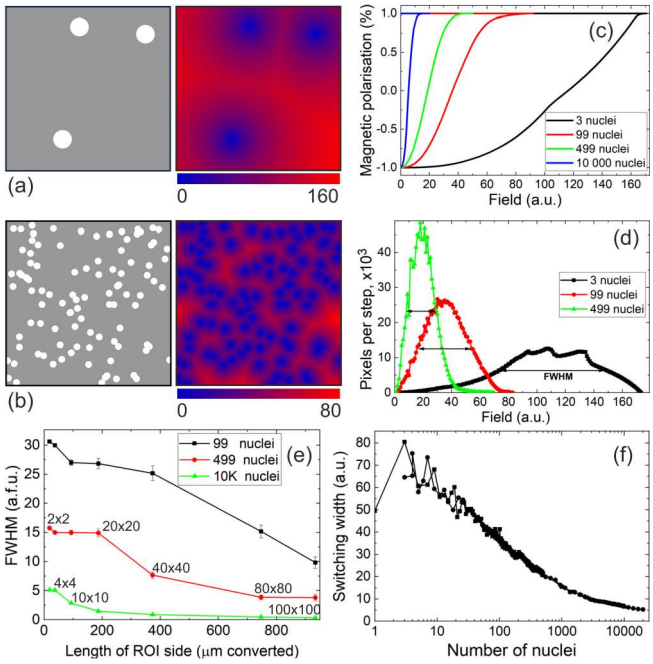


FIGURE 3. Modelling of domain evolution (area of 1000×1000 pixels): magnetic bubble domains and coercive field distribution for different nuclei numbers, exemplarily shown for 3 **(a)** and 99 **(b)** pixels. **(c)** Global hysteresis loops for different nuclei number and **(d)** the amount of sample area switched per field step for the correspondent loops. **(e)** The FWHM of the pixel switching distribution as a function of the region size for local analysis for 99, 499, and 10.000 nuclei and **(f)** as a function of nuclei number obtained with 2×2 pixel binning.

also corresponds to approximately 5-10 nuclei within the ROI. This leads us to assume that the minimum number of domain nucleation sites that should be observable in the field of view is at least five. At this density, the nucleated domains are sufficiently close to each other so that their expansion covers the entire ROI within an external field change of less than 1% of the global $H_{C,G}$, effectively converging the local measurement toward the macroscopic coercive field.

To validate those experimental results, we performed computer modelling of bubble domain nucleation and evolution for various numbers of nuclei ranging from 1 to $2{\cdot}10^4$, generated randomly within a square of size $10^3 \times 10^3$ pixels, which is rather close to the total domain image size obtained in the experiments thus allowing for their direct comparison. The simulation follows a discrete step-by-step algorithm. At each iteration i, every nucleation center acts as the origin of an expanding circle with radius R_i. A pixel is considered as switched if it falls within the radius of at least one expanding domain. To ensure the model's reliability, we assume: (i) uniform nucleation, where all domains start growing simultaneously at $i = 0$ from randomly assigned coordinates; (ii) isotropic growth, meaning the domain wall velocity is identical in all directions, resulting in perfectly circular expansion until the domains encounter each other or the sample boundaries; and (iii) edge effects, accounted for by applying open boundary conditions where domains reaching the edge of the simulation grid cease to expand,

accurately reflecting the finite field of view in MOKE experiments. At each iteration step of bubble evolution, the bubble radius is increased by one pixel, causing the pixels with coordinates within the enlarged radius to be considered as switched. To account for the increasing bubble growth speed with increasing field amplitude, we implemented an iteration-dependent correction coefficient 1.01^i, where i is the iteration number, so that the bubble radius depends on an iteration step as $R_{i+1} = 1.01^i \cdot R_i$. This step-by-step radial expansion phenomenologically emulates the magnetization reversal via domain wall propagation from a finite number of nucleation sites, a well-established mechanism for ultrathin films with perpendicular magnetic anisotropy [12]. Furthermore, the exponential acceleration factor (1.01^i) reflects the non-linear field dependence of the domain wall velocity during a continuous field sweep, consistent with the dynamic behavior reported in earlier literature [12]. In Figs. 3, the bubble domains during their evolution are presented by example of 3 (Fig. 3a) and 99 (Fig. 3b) nuclei, together with the spatial distribution of the local switching fields, corresponding individual global magnetization switching curves (Fig. 3c), and the dependence of pixels switched per step (Fig. 3d). In this diagram, zero field corresponds to the nucleation field, i.e., the field at which magnetization reversal begins. The distortions at the top of the black curve in Fig. 3d, which can also be seen in real samples (plateau in Fig.2a, black curve), are attributed to the situation when the domain walls of a some bubbles reach the sample edge and stop growing in that particular direction. As seen, the behaviour of the modelled bubble domains is very similar to that experimentally observed in our three Co/Pt films with corresponding numbers of nuclei.

Figure 3e shows the dependence of the modelled FWHM on the ROI size for three exemplary cases with 99, 499, and 10,000 nuclei, which correspond to 1.13, 5.72, and 114.6 nuclei/mm^2 (assuming a pixel size of 9.34 μm like in the experiment). As in the experiment, with increasing ROI size at the lowest nucleation density, the width of the switching field distribution decreases only slowly without any signs of flattening. At higher densities, following a plateau at low pixel binning values, there is a sharp drop followed by a slow decline. For the 499-nuclei curve, such a drop is observed at 80×80 pixel binning, which corresponds to approximately 3 nuclei within this ROI (747×747 μm^2), and for the 10,000-nuclei curve, the drop occurs at 20×20 pixel binning, corresponding to approximately 4 nuclei within the ROI (186×186 μm^2). These values match their experimental counterpart of 5 nuclei within the ROI, required for a reasonable extrapolation of locally measured sample properties to the global scale.

The dependence of the FWHM of sample switching on the number of nucleation centers, obtained from the modeled data with 2×2 pixel binning and shown in Figure 3f, reveals the expected trend: the switching width decreases as the number of nuclei increases. Once the number of nuclei exceeds approximately 10^3, a noticeable change in the slope of the curve is observed, suggesting a minimum required nuclei number for the correct interpretation of magnetometry data.

From these experimental and modelled observations, we can now draw an important conclusion about the measurement of hysteresis curves on PMA layers using MOKE magnetometry with regard to their relevance for characterizing complete film samples: The typical laser spot size used in *laser-based* MOKE magnetometry is 10-100 μm for standard and 1-10 μm for high-resolution setups, so that the obtained MOKE hysteresis curves will always have some local character. To ensure that such local curves are also relevant to the entire sample, a minimum number of domain nuclei must be detected within the laser spot as elaborated. Taking into account our determined minimum nuclei number of 5, we estimate the required minimum nuclei density for a 100 μm spot to be ∼500 nuclei/mm^2 and for a 10 μm spot to be $\sim 5 \cdot 10^4$ nuclei/mm^2. This would mean that $\sim 3.2 \cdot 10^4$ and $\sim 3.2 \cdot 10^6$ nuclei, respectively, must be present in a sample of 8×8 mm size as used in our experiment. This implies that great care should be taken when interpreting MOKE loops obtained in a laser-based MOKE system. If, on the other hand, the curves are measured in a wide-field microscope, there is much greater leeway in choosing the spot (ROI) size for data analysis, making it easier to meet the requirement of detecting the minimum number of nuclei and thus obtaining more reliable hysteresis curves and coercive fields.

IV. TEMPORAL ASPECTS OF HYSTERESIS LOOPS

Magnetic hysteresis refers to the delay in the magnetization response of a sample following the application of a magnetic field. When the field changes, the magnetization does (in general) not follow immediately but its reaction depends on the previous magnetic state. In terms of temporal behavior, there are two regimes: *time-independent* (quasistatic) hysteresis, which arises from structural imperfections in the material (e.g., defects, grain boundaries, and internal stress), and *time-dependent* (dynamic) hysteresis, which occurs when the field changes rapidly, causing additional retardation of domain wall motion due to eddy currents, magnetic viscosity, or other relaxation processes [15].

When the magnetic field increases gradually, domain walls do not move smoothly but rather jump discontinuously from one pinning site to another known as Barkhausen jumps. The macroscopic magnetic hysteresis loop is the cumulative result of numerous Barkhausen jumps occurring throughout the material. Time-*independent* hysteresis represents the average outcome of these microscopic domain wall jumps and reflects the distribution of pinning barriers — stronger pinning leads to a wider hysteresis loop and fewer, but larger jumps. Time-*dependent* hysteresis, on the other hand, modifies the dynamics of these jumps: when the field changes rapidly, the walls cannot respond instantaneously, leading to delayed or smeared-out jumps, viscous losses, and additional loop broadening.

The usual way to measure a hysteresis loop by magneto-

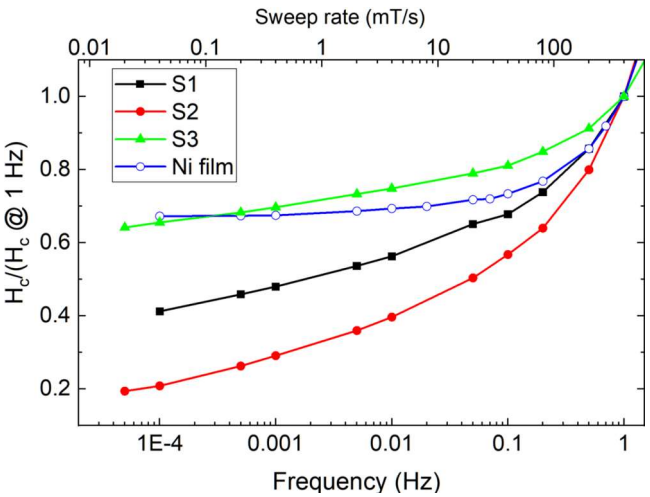


FIGURE 4. Coercivity of the entire sample areas as a function of frequency of an applied triangular AC field of 100 mT amplitude. While for the in-plane magnetized, 20 nm thick nickel film (blue curve) H_c reaches saturation below 100 mHz, all three Co/Pt films with out-of-plane anisotropy reveal no signatures of leveling off down to 5 μHz.

optical means is either (i) to apply an alternating magnetic field with a frequency of a few Hertz and track the intensity of the Kerr signal (as is often the case with laser-based magnetometry) or (ii) stepping through the field and plotting the average ROI image gray value as a function of the applied field (as is typically done in microscopy-based magnetometry). When the sweeping rate of the external magnetic field is sufficiently low, the quasistatic regime is realized and the hysteresis measurement may provide access to sample properties. However, the field rate that grants the quasistatic limit may differ significantly for different materials, making the speed of the loop recording a major factor in appropriate sample characterization.

To investigate the influence of the field sweep rate on the hysteresis loop parameters, we recorded magnetization reversal loops (over the whole sample area) of our three Co/Pt samples in a magnetic field ramped at different speeds (Fig. 4). As a reference, the same experiments were repeated on a nickel thin film (40 nm film on Si substrate) with in-plane anisotropy and applied in-plane magnetic field (using the longitudinal Kerr effect). All three Co/Pt films exhibit a similar trend: despite the presence of multiple nucleation centers, coercivity continues to decrease linearly as $\log_{10}(\nu)$ at low frequencies, with no quasistatic plateau observed. In contrast, the nickel film shows a substantially different response: below 10 mHz, the coercive field dependence flattens out, reaching the frequency-independent quasistatic regime.

Such a difference in behaviour can be attributed to the different domain wall propagation conditions in these two materials. In Co/Pt, the domain walls normally proceed in the *creep* regime[3], and significant collective pinning of domain walls hinders the complete relaxation even at very low field change rates, whereas in nickel, with its in-plane anisotropy and weak pinning, domain walls propagate in the *flow* regime. This allows domain walls to overcome local energy barriers during slow field variation, resulting in a frequency-independent coercivity that reaches the quasistatic plateau. Frequency-dependent coercive fields have already been observed in thin films with in-plane [16], [17] and out-of-plane [18]–[20] anisotropy, with emphasis on higher frequencies where the coercive field appears to saturate in the low-frequency range. Looking now at this low-frequency range for our Co/Pt films, it becomes clear that saturation is not reached even at very low sweep rates (Fig. 4), which means that the absolute value of the coercive field strength must be always treated with extreme caution, i.e., regardless of the more or less local character of MOKE magnetometry.

[3]In PMA films, dominated by domain wall creeping, the walls continue their movement even when the applied magnetic field is stopped.

CONCLUSIONS

Using the example of Co/Pt thin films with perpendicular anisotropy, which are magnetized by the nucleation of bubble domains and their growth through wall motion, we have investigated an aspect of MOKE magnetometry that is often ignored when this method is used to measure magnetic hysteresis loops in perpendicularly magnetized, extended film media: The loop coercive force depends strongly on the probe size of the magnetometer. Using computer modelling, we have found that at least five domain nuclei must be present within the measurement spot in order to obtain loops that resemble those of a complete film sample. Otherwise, the MOKE loops are only local in nature with a broad distribution of coercive fields, so that no accurate conclusions can be drawn about the entire sample. From this point of view, MOKE magnetometry performed in a wide-field polarization microscope has a clear advantage over laser-based magnetometers, as it allows easy adjustment of the spot size by choosing a suitable objective and selecting suitable areas for Kerr intensity analysis. In any case, however, domain wall creep effects can have a significant influence on the measured coercive field strength, an aspect that should not be ignored, not only in MOKE magnetometry.

REFERENCES

[1] W. Kuch, R. Schäfer, P. Fischer, and F. U. Hillebrecht, Magnetic microscopy of layered structures. Springer Science & Business Media, 2015.
[2] J. McCord, N. O. Urs, and M. Vogel, "Perspectives on magneto-optical microscopy techniques," Applied Physics Letters, vol. 127, no. 18, p. 180501, 11 2025. [Online]. Available: https://doi.org/10.1063/5.0288840
[3] R. Schäfer and J. McCord, Magneto-Optical Microscopy. Cham: Springer International Publishing, 2021, pp. 171–229.
[4] I. Soldatov and R. Schäfer, "Advanced MOKE magnetometry in wide-field Kerr-microscopy," J. Appl. Phys., vol. 122, p. 153906, 2017.
[5] A. Hubert and R. Schäfer, Magnetic Domains: The Analysis of Magnetic Microstructures. New York: Springer, 1998.
[6] T. Huang, J. Dong, T. Huang, T. Mei, L. Hu, C.-H. Lin, F. Chen, D. Chu, Z. Cheng, and Z. Li, "Advancing characterization for magnetic materials via magneto-optical kerr effect microscopy," Small, vol. 22, no. 5, p. e10608, 2026. [Online]. Available: https://onlinelibrary.wiley.com/doi/abs/10.1002/smll.202510608
[7] D. Marko, I. Soldatov, M. Tekielak, and R. Schäfer, "Stray-field-induced Faraday contributions in wide-field Kerr microscopy and -magnetometry," J. Magn. Magn. Mat., vol. 396, pp. 9–15, 2015.

[8] W. Rave and A. Hubert, “Refinement of the quantitative magnetooptic domain observation technique,” IEEE Trans. Magn., vol. 26, pp. 2813–2815, 1990.
[9] I. Soldatov and R. Schäfer, “Selective sensitivity in Kerr microscopy,” Rev. Scient. Instr., vol. 88, p. 073701, 2017.
[10] J. Kranz and B. Passon, “Messung der Magnetisierung in der Oberflaeche von Eisen-Silizium-Einkristallen mit Hilfe des vergrösserten magnetooptischen Kerr-Effektes,” Zeitschrift Angewandte Physik, vol. 13, no. 3, pp. 122–124, 1961.
[11] I. Soldatov, P. Andrei, and R. Schäfer, “Inverted Hysteresis, Magnetic Domains, and Hysterons,” IEEE Magn. Lett., vol. 11, pp. 1–5, 2020. [Online]. Available: 10.1109/LMAG.2020.3035136
[12] A. Kirilyuk, J. Ferré, V. Grolier, J. Jamet, and D. Renard, “Magnetization reversal in ultrathin ferromagnetic films with perpendicular anisotropy,” Journal of Magnetism and Magnetic Materials, vol. 171, no. 1, pp. 45–63, 1997. [Online]. Available: https://www.sciencedirect.com/science/article/pii/S0304885396007445
[13] J. Ferré, V. Grolier, P. Meyer, S. Lemerle, A. Maziewski, E. Stefanowicz, S. V. Tarasenko, V. V. Tarasenko, M. Kisielewski, and D. Renard, “Magnetization-reversal processes in an ultrathin co/au film,” Phys. Rev. B, vol. 55, pp. 15 092–15 102, Jun 1997. [Online]. Available: https://link.aps.org/doi/10.1103/PhysRevB.55.15092
[14] Y. Iunin, Y. Kabanov, V. Nikitenko, X. Cheng, A. Shapiro, C. Chien, and R. Shull, “On the nature of asymetry of nucleation centers activity in ultrathin co films and co/pt multilayers,” Functional Materials, vol. 15, no. 1, p. 51, 01 2008.
[15] G. Bertotti, Hysteresis in Magnetism: For Physicists, Materials Scientists, and Engineers. San Diego: Academic Press, 1998.
[16] J.-S. Suen and J. L. Erskine, “Magnetic Hysteresis Dynamics: Thin $p(1 \times 1)$ Fe Films on Flat and Stepped W(110),” Phys. Rev. Lett., vol. 78, pp. 3567–3570, May 1997. [Online]. Available: https://link.aps.org/doi/10.1103/PhysRevLett.78.3567
[17] K. Toyoki, S. Matsui, Y. Shiratsuchi, Y. Endo, and R. Nakatani, “Frequency dependence of coercivity in nickel and Co-Fe-B thin film for DC to 100 kHz region,” Japanese Journal of Applied Physics, vol. 62, no. SB, p. SB1008, nov 2022. [Online]. Available: https://doi.org/10.35848/1347-4065/ac918a
[18] P. Bruno, G. Bayreuther, P. Beauvillain, C. Chappert, G. Lugert, D. Renard, J. P. Renard, and J. Seiden, “Hysteresis properties of ultrathin ferromagnetic films,” Journal of Applied Physics, vol. 68, no. 11, pp. 5759–5766, 12 1990. [Online]. Available: https://doi.org/10.1063/1.346944
[19] A. Mardana, S. Ducharme, and S. Adenwalla, “The sweep rate dependence of the electrical control of magnetic coercivity,” Journal of Applied Physics, vol. 111, no. 7, p. 07C708, 02 2012. [Online]. Available: https://doi.org/10.1063/1.3673829
[20] G. Vértesy and A. Magni, “Frequency dependence of coercive properties,” Journal of Magnetism and Magnetic Materials, vol. 265, no. 1, pp. 7–12, 2003. [Online]. Available: https://www.sciencedirect.com/science/article/pii/S0304885302015779



DR. IVAN SOLDATOV received his B.Sc. and M.Sc. degrees in Solid State Physics from Ural State University, Yekaterinburg, Russia, in 2007 and 2009, respectively. He earned his Ph.D. in Physics from the Technische Universität Dresden, Germany, in 2016, with a dissertation titled "Thermoelectric Effects and Anisotropy in Magnetic Films."

From 2005 to 2011, Dr. Soldatov worked as a Research Fellow at Ural State University, where he focused on charge transport effects in low-dimensional semiconductor systems. Since 2011, when he joined the Leibniz Institute for Solid State and Materials Research, Dresden, Germany, he has worked as a Research Fellow, specializing in magneto-optical Kerr microscopy, magnetic domains, and overseeing various research grants.

From 2021 to 2022, Dr. Soldatov took a leave from IFW, working as a Team Leader in the Functional Materials group at the Technical University of Darmstadt, where he led research in permanent magnets and domain imaging. He also served as an Application Engineer at KLA-Tencor, Dresden, providing customer support and tool commissioning in metrology-related projects.

His field of interest encompasses a broad range of magnetic materials, with a focus on magnetic domain observation using wide-field magneto-optical Kerr microscopy. He has published more than 80 articles in peer-reviewed journals, including a book chapter. In addition to his scientific activities, he is dedicated to advancing and improving the methodology of Kerr microscopy.



AMAN SINGH received his B.Sc. and M.Sc. degrees in Physics from University of Delhi and Indian Institute of Technology Delhi, India, in 2020 and 2022, respectively. In 2023, he joined Leibniz IFW Dresden, Germany as a Ph.D. candidate in the ‘Magnetic Microscopy and Thin Film Devices’ group. His current research focuses on tailoring ferroic textures in thin films via geometrical transformation.



VOLKER NEU received his Diploma degree in physics from the Karlsruhe Institute of Technology, Karlsruhe, Germany, in 1993, and the Ph.D. degree from the Dresden University of Technology, Dresden, Germany, in 1998. He then worked as a postdoctoral researcher for one and a half years at the Center for Materials Research and Technology (MARTECH), Florida, USA, before returning to Germany in 1999 as a postdoctoral researcher at the Leibniz Institute for Solid State and Materials Research Dresden (IFW Dresden). Since 2003 he holds a permanent position at IFW Dresden as a group leader for Magnetic Microscopy and Magnetic Thin Film Devices, working on thin film development, device fabrication, tailoring magnetic textures, and nanoscale quantitative MFM (qMFM). He has published more than 150 articles in per-reviewed journals.



RUDOLF SCHÄFER (M'08–SM'18) received the diploma degree in materials science and the Ph.D. degree in engineering from the University of Erlangen-Nürnberg, Germany, in 1985 and 1990, respectively. He then joined the IBM Research Center in Yorktown Heights, USA, and the Forschungszentrum Jülich, Germany, as a Postdoctoral Researcher in 1991 and 1992, respectively. In 1993 he moved to the IFW Dresden where he became head of the Department of Magnetic Microstructures in 2002. In 2011, he was appointed Adjunct Professor for Magnetic Materials at the Institute for Materials Science, Technical University Dresden.

His areas of interest span magnetic materials with a focus on magnetic microstructures and domain imaging by Kerr microscopy. He has published more than 250 technical articles in peer-reviewed journals, including book chapters, and he has coauthored the Springer textbook Magnetic Domains together with Alex Hubert.

Prof. Schäfer was member of the Technical Committee of IEEE Magnetics Society from 2008 to 2014 and member of the societies Conference Executive Committee from 2015 to 2024, serving as its chair from 2017 to 2024. In 2013 he was elected Distinguished Lecturer of the IEEE Magnetics Society. He furthermore is director of the evico magnetics GmbH.